Colossal Magnetoresistance Manganite Perovskites: Relations between Crystal Chemistry and Properties

B. Raveau,* A. Maignan, C. Martin, and M. Hervieu

Laboratoire CRISMAT, UMR 6508/CNRS, ISMRA and University of Caen, 6, Boulevard du Maréchal Juin, 14050 Caen Cedex, France

Received March 24, 1998. Revised Manuscript Received June 1, 1998

Manganites with the perovskite structure represent a very important family of oxides which are extensively studied for their colossal magnetoresistance (CMR) properties. In the present review we discuss the different factors which govern the magnetic and transport properties of these materials: carrier concentration, average size of the interpolated cation, and mismatch effect on the A-site. Three types of oxides are mainly examined: (i) the hole doped manganites $Ln_{0.7}A_{0.3}MnO_3$ (A = Ca, Sr, Ba), (ii) the "charge ordered" $Ln_{0.5}A_{0.5}MnO_3$ manganites, and (iii) the electron doped manganites $Ca_{1-x}Ln_xMnO_3$ and $Ca_{1-x}Th_xMnO_3$. The relationships between structural and magnetic transitions are discussed, and particular attention is paid to charge ordering phenomena. The doping of the Mn sites by various elements (Al, Ga, In, Ti, Sn, Fe, Cr, Co, Ni) is systematically examined. The beneficial effect of "Cr, Co, Ni" elements, which induce CMR properties in these perovskites, is emphasized.

Contents

Introduction

Manganese oxides with the perovskite structure have been the subject of numerous papers since the discovery of large magnetoresistance in these materials.[1,2] These manganites with the generic formulation $Ln_{1-x}A_xMnO_3$ (A = Ca, Sr, Pb, Ba) exhibit a decrease of the resistance on applying a magnetic field near their Curie temperature (T_C) so that their magnetoresistance MR is negative and generally defined as $MR = \Delta R/R_0 = (R_H - R_0)/R_0$ [see for review refs 3 and 4]. Recent investigations have shown that, for these oxides, MR tends toward 100%,[5−18] so that the amplitude of the effect is better evidenced by the RR ratio $RR = R_0/R_H$, which can reach extremely high values, up to 10^{11}. For this reason, these compounds have been named CMR (colossal magnetoresistance) manganites.

An overview of the CMR effect in the manganites has been given previously,[3] so that the fundamental effect is supposed to be well-known by the reader. In contrast, the mechanism of the CMR effect is so far not completely understood. Although we know that it is based on the double exchange (DE) between the Mn^{3+} and Mn^{4+} species,[19−21] the role of Jahn−Teller-type electron−phonon interactions has only been shown recently.[22] Moreover charge ordering phenomena have to be taken into consideration which are susceptible to influencing dramatically the CMR properties of these materials. Thus, at this point of the investigation we have to understand the issues concerning the role of the manganese mixed valence, the effect of the size and of the disordering−ordering of the A site cations, and the role of charge ordering and of the structural transitions upon the properties of these manganites. In the present paper, we review the relationships between the solid-state chemistry of the manganites and their CMR properties, emphasizing the progress made these past 2 years.

Hole Doped CMR Manganites $Ln_{0.7}A_{0.3}MnO_3$ and $Ln_{0.66}A_{0.34}MnO_3$

Among the perovskites $Ln_{1-x}A_xMnO_3$, with A = Ca, Sr, Ba, Pb and Ln being a lanthanide, those for which $x \sim 0.30$ exhibit considerable magnetoresistances. This is for instance the case of the manganites $Pr_{0.7}Ca_{0.30-x}Sr_xMnO_3$ whose resistance can be decreased by 4−11 orders of magnitude on applying a magnetic field of 6 T.[23] For instance for $x = 0.05$ one observes a maximum at 90 K (T_{max}) on the $R(T)$ curve in a zero magnetic field (Figure 1a), which corresponds to an insulator−metal transition as T decreases, whereas under 5 T the $R(T)$ curve is dramatically flattened (Figure 1a), showing a R_0/R_{5T} ratio of 2×10^5. As shown for the $M(T)$ curve registered under 1.45 T (Figure 1b), this transition coincides with a paramagnetic to ferromagnetic transition as T decreases. Thus, in a general way, the CMR manganites are characterized by a paramagnetic insulator (PMI) to ferromagnetic metallic (FMM) transition as T decreases. Note however that the existence of the insulator−metal transition is not necessary for the appearance of CMR. This is il-

10.1021/cm9801791 CCC: $15.00
Published on Web 09/19/1998

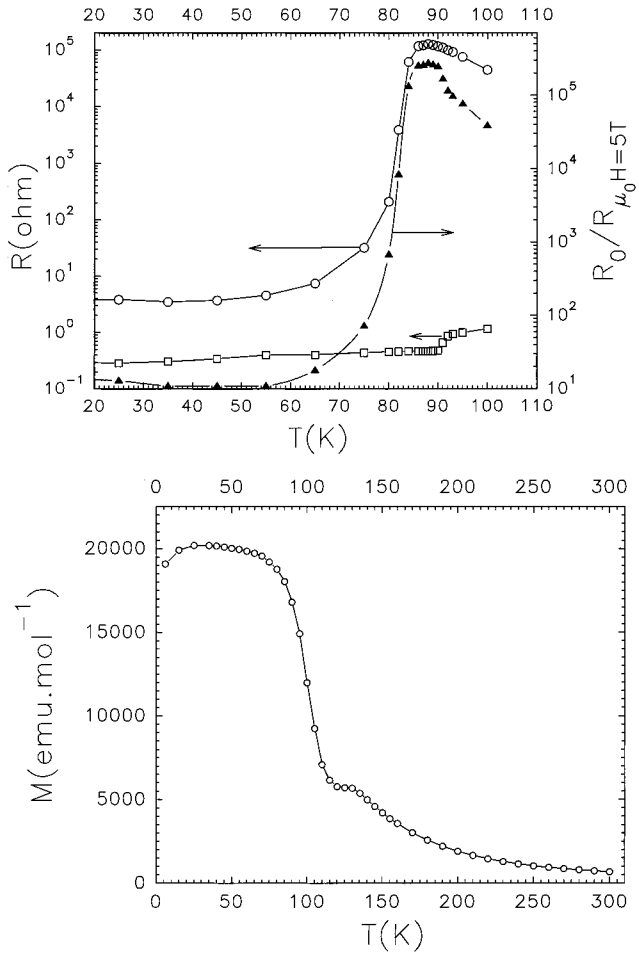

Figure 1. (a, top) T dependence of the resistance (R) for the ceramic $Pr_{0.7}Ca_{0.25}Sr_{0.05}MnO_3$: (○) $B = 0$, (□) $B = 5$ T, and (▲) R/R_{5T}. (b, bottom) Corresponding magnetization (M) versus T curve.

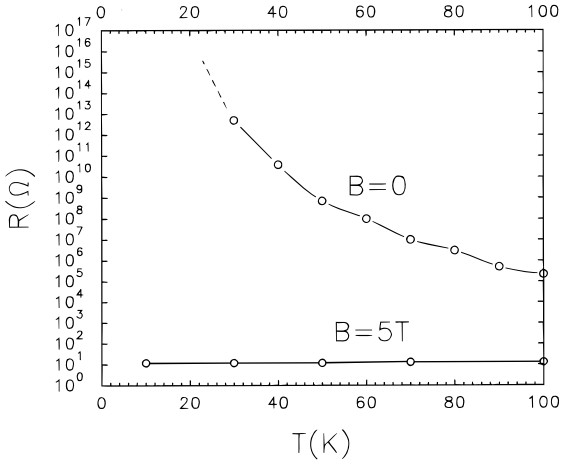

Figure 2. $R(T)$ curves of $Pr_{0.7}Ca_{0.26}Sr_{0.04}MnO_3$.

lustrated for $Pr_{0.7}Ca_{0.26}Sr_{0.04}MnO_3$,[16] which exhibits a semiconducting behavior in a zero magnetic field and becomes a ferromagnetic metal under 5 T (Figure 2) so that a resistance ratio of 10^{11} is reached for this phase.

Two parameters must be taken into consideration to explain the magnetotransport properties of these oxides: the hole carrier density and the overlapping of the manganese and oxygen orbitals. The hole concentration is provided by the amount of tetravalent manganese introduced in the trivalent manganese perovskite $LnMnO_3$, by just replacing partly the trivalent lanthanide cation Ln^{3+} by a divalent cation A^{2+}. Thus, the hole carrier density is controlled by the Mn(III)/Mn(IV) ratio. The overlapping of the Mn 3d orbitals and O 2p orbitals depends on the Mn−Mn distance between two consecutive MnO_6 octahedra and on the Mn−O−Mn angle. It can be modified by varying the size of the interpolated cation (A, Ln). The effect of the average size of the interpolated cation has been studied by several groups.[9,13,16−18,24−29] The $R(T)$ curves (Figure 3a) and $M(T)$ curves (Figure 3b) of the manganites $Pr_{0.7}Ca_{0.3-x}Sr_xMnO_3$,[24] characterized by a fixed Mn(III)/Mn(IV) ratio, show clearly the effect of the average size of the ionic radius $\langle r_A \rangle$ of the interpolated cation (Ln, Sr, Ca) upon the magnetotransport properties of these oxides. One indeed observes that the Curie temperature T_C (Figure 3b), which coincides with the metal−insulator (MI) transition at T_{max} (Figure 3a), increases regularly as x increases, i.e., as $\langle r_A \rangle$ increases. Moreover, the resistance ratio for $R_{T_{max}}/R_{(10K)}$ decreases significantly as x increases, from 3×10^4 for $x = 0.05$ to 170 for $x = 0.10$. In fact, the graph T_m ($\langle r_A \rangle$), plotted in Figure 4 for this series, shows that for a constant hole carrier density (0.3 hole/Mn mole), T_C increases dramatically and almost linearly as $\langle r_A \rangle$ increases. The effect of the hole carrier density can be evaluated by comparing the above series with the oxides $Pr_{0.66}Ca_{0.34-x}Sr_xMnO_3$ (Figure 4),

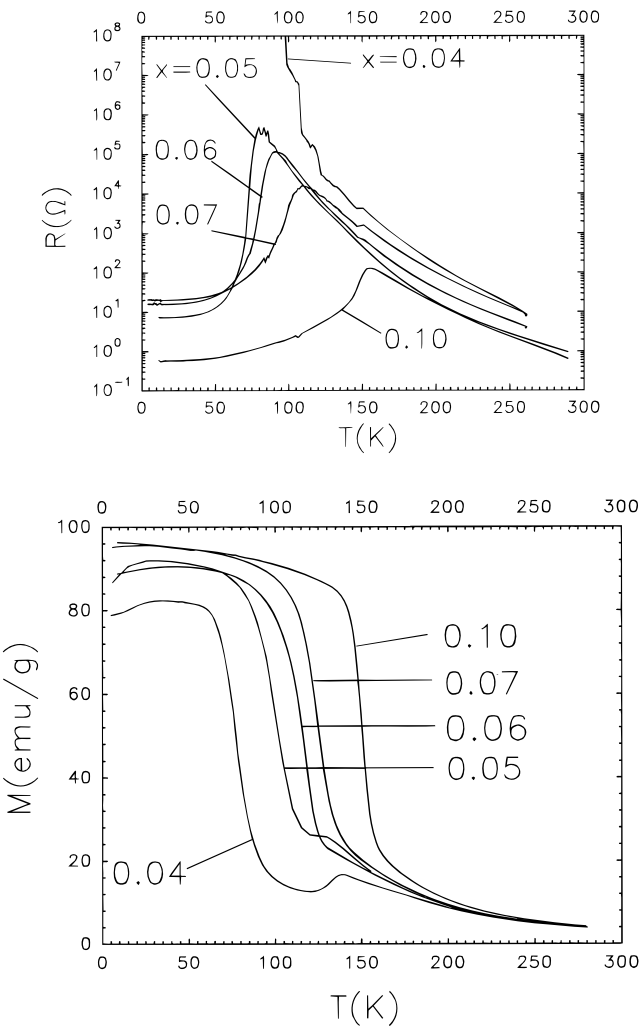

Figure 3. (a, top) $R(T)$ curves of the $Pr_{0.7}Ca_{0.30-x}Sr_xMnO_3$ series. (b, bottom) Corresponding $M(T)$ curves.

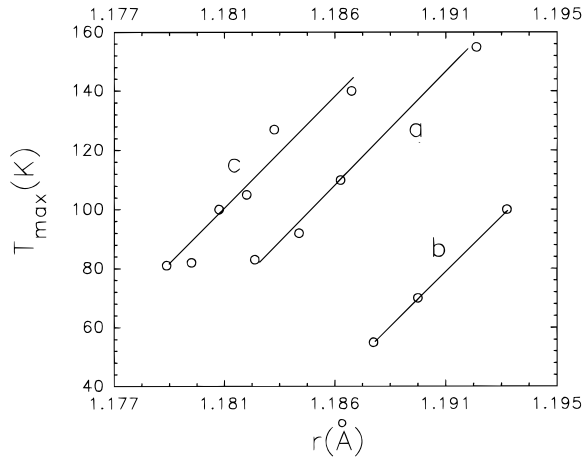

Figure 4. T_{max} ($R(T)$ maximum value) versus $\langle r_A \rangle$ for the series (a) $Pr_{0.7}Ca_{0.30-x}Sr_xMnO_3$, (b) $Pr_{0.66}Ca_{0.34-x}Sr_xMnO_3$, and (c) $Pr_{0.7-x}La_xCa_{0.3}MnO_3$.

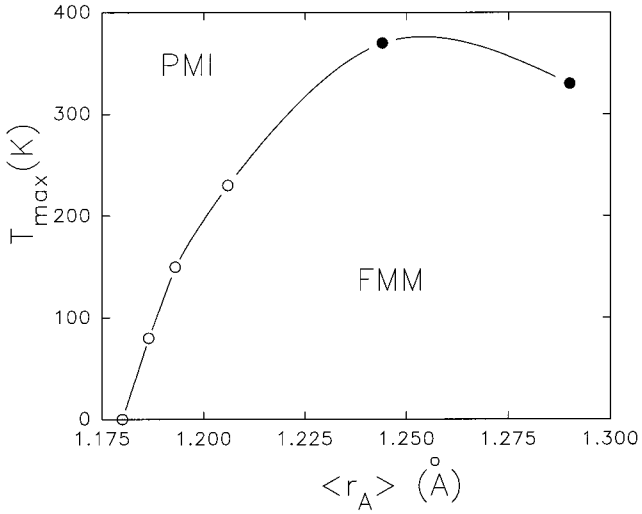

Figure 5. $\langle r_A \rangle$ dependence of T_{max} for the $Ln_{0.7}A_{0.3}MnO_3$ manganites: (○) data from ref 18 and (●) data from ref 31.

which exhibit a different hole carrier density (0.34 hole/Mn). We notice that this second series also exhibits a linear increase of T_C as $\langle r_A \rangle$ increases. But most important is the fact that for a same $\langle r_A \rangle$ value, each oxide of the series $Pr_{0.66}Ca_{0.34-x}Sr_xMnO_3$ exhibits a T_C 70 K smaller than the corresponding oxide of the series $Pr_{0.7}Ca_{0.3-x}Sr_xMnO_3$.

The linear increase of T_C versus $\langle r_A \rangle$ has been generalized to several other manganites such as $Pr_{0.7-x}La_xCa_{0.3}MnO_3$,[24] $La_{0.7-x}Y_xCa_{0.3}MnO_3$,[30] and $Nd_{0.7}Ca_{0.3-x}Sr_xMnO_3$.[26] From considerations of this size effect, magnetic phase diagrams have been established for different series of manganites.[31−33] This is illustrated by the diagram T_C ($\langle r_A \rangle$) (Figure 5) for the series $Ln_{0.7}A_{0.3}MnO_3$. One can see that T_C (or T_{max}) increases abruptly and almost linearly for 1.19 Å < $\langle r_A \rangle$ < 1.24 Å, in agreement with the above statements. However, one observes that T_{max} goes through a maximum value of 360 K at $\langle r_A \rangle$ = 1.24 Å, decreasing on the right side as $\langle r_A \rangle$ increases further. In the same way, below $\langle r_A \rangle$ = 1.19 Å, T_C does not vary so dramatically and moreover the FMM state disappears at the benefit of the FMI (ferromagnetic insulating) state.[31] Note that for $\langle r_A \rangle$ = 1.18 Å, which corresponds to the $\langle r_A \rangle$ value of $Pr_{0.7}Ca_{0.3}MnO_3$, the CMR effect tends to disappear in agreement

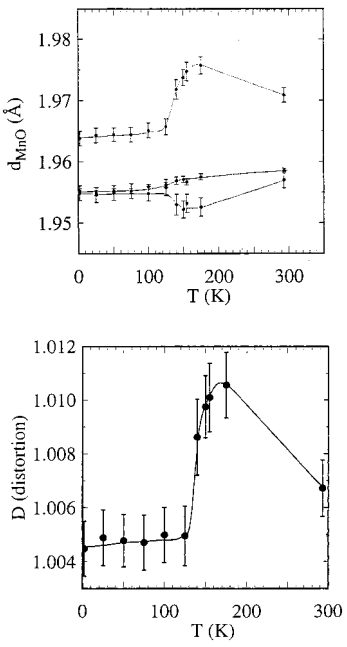

Figure 6. (a, top) T dependence of the Mn−O distances for $Pr_{0.7}Ca_{0.2}Sr_{0.1}MnO_3$. (b, bottom) Jahn−Teller distortion ($d_{Mn-O_{apical}}/d_{Mn-O_{equatorial}}$).

with the decrease of magnetization with $\langle r_A \rangle$.[24] The disappearance of the FMM state at low $\langle r_A \rangle$ has been explained by the decrease of the Mn−O−Mn angle with $\langle r_A \rangle$, making the bandwidth more narrow.[22]

The disappearance of linearity in T_C ($\langle r_A \rangle$) for high $\langle r_A \rangle$ values in the ferromagnetic regime (Figure 5) shows that, besides the size effect, there exists another factor which influences strongly T_C. Rodriguez-Martinez and Attfield[34] have indeed shown that the disordering of Ln^{3+} and A^{2+} cations on the A-site contributes dramatically to the decrease of T_C in the $Ln_{0.7}A_{0.3}MnO_3$ manganites. They have demonstrated that for the same A-site average size $\langle r_A \rangle$ = 1.23 Å, T_C decreases as the size difference between the A-site cations increases. To quantify this effect, called mismatch, they have introduced the σ^2 variance of the A cations radii distribution, $\sigma^2 = \sum y_i r_i^2 - \langle r_A \rangle^2$, where y_i are the fractional occupancies of the different A cations of r_i radii. For instance in a comparison of $La_{0.70}Ca_{0.11}Sr_{0.19}MnO_3$ and $Sm_{0.70}Ba_{0.30}MnO_3$, which have the same $\langle r_A \rangle$ and the same hole carrier density but very different σ^2 of 16×10^{-4} and 24×10^{-3} Å^2, respectively, they show that T_C decreases from 360 to 60 K, demonstrating the crucial mismatch effect on the magnetotransport properties of these oxides. Thus the magnetic phase diagrams T_C ($\langle r_A \rangle$) do not render an account of the size effect only, and the antagonist mismatch effect must be taken into consideration.

To explain the magnetotransport properties of the manganites, we have to determine whether the magnetic transitions are related to structural transitions. The role of the Jahn−Teller effect of manganese, as well as charge ordering phenomena in these mangnetotransport properties, are issues that have to be answered to understand the CMR mechanisms.

The neutron powder diffraction (NPD) study of the manganite $Pr_{0.7}Ca_{0.2}Sr_{0.1}MnO_3$ which exhibits a PMI−FMM transition at 170 K[35] sheds light on these relationships between structure and properties. One ob-

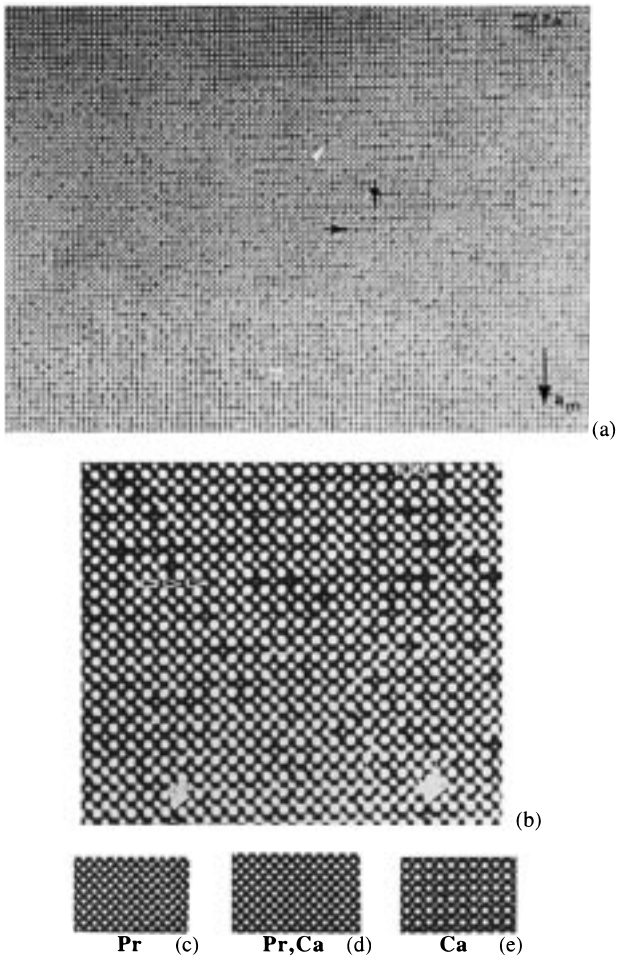

Figure 7. Typical $[101]_p$ images: (a) overall and (b) enlarged images of point like defects in $Pr_{0.7}Ca_{0.25}Sr_{0.05}MnO_3$. Comparison between the calculated images for (c) $PrMnO_3$, (d) $Pr_{0.7}Ca_{0.25}Sr_{0.05}MnO_3$, and (e) $CaMnO_3$.

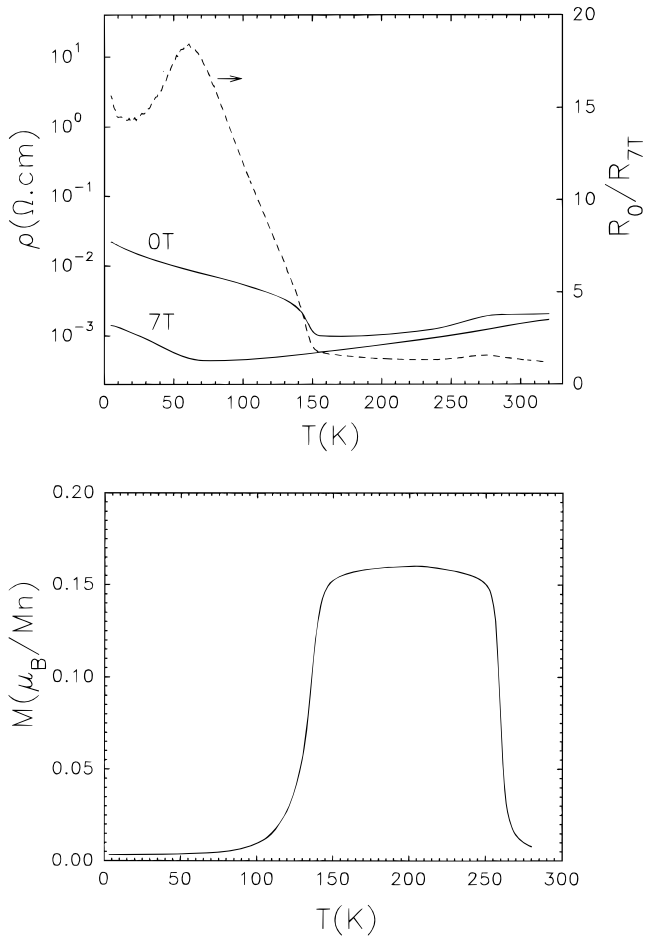

Figure 8. (a, top) $\rho(T)$ curves of $Pr_{0.5}Sr_{0.5}MnO_3$. (b, bottom) Corresponding $M(T)$ curve registered under 100 G.

serves a significant contraction of the lattice below the FMM transition. An abrupt variation of the Mn−O distances is observed at the transition (Figure 6a). In the PMI state, the Jahn−Teller distortion increases as T decreases. One observes elongated octahedra with two larger apical bonds (1.971−1.976 Å) and four shorter equatorial bonds (1.958−1.952 Å). In the ferromagnetic state, the distortion still exists but does not vary significantly at low temperature, with two apical distances of 1.96 Å and four equatorial distances ranging from 1.955 to 1.966 Å. Clearly, the PMI to FMM transition coincides exactly with the decrease of the Jahn−Teller distortion (Figure 6b). A rather similar decrease of the Jahn−Teller distortion below T_C has also been observed in the canted ferromagnetic insulator $La_{0.875}Sr_{0.125}MnO_3$ by Argyriou et al.[36] Although they correspond to a static effect, these correlations between the Jahn−Teller distortion and magnetic ordering of manganese are in agreement with the theory developed by Millis et al.,[22] which emphasizes the important role of the dynamic Jahn−Teller effect in the properties of these materials. But the high-resolution electron microscopy (HREM) study of this phase at room temperature[37] shows that the relationship between structure and properties is certainly more complex than expected from NPD data. The NPD study of $Pr_{0.70}Ca_{0.25}Sr_{0.05}MnO_3$[38] has indeed evidenced for this phase an orthorhombic symmetry "$a_p\sqrt{2} \times 2a_p \times a_p\sqrt{2}$" and space group $Pnma$, whereas HREM observations show the existence in this matrix of monoclinic domains ($a_m \sim 2a_p$, $b_m \sim a_p\sqrt{2}$, $\beta \sim 90.3°$), whose structure can be simulated in the space group $P2_1/c$. Moreover the $[101]_0$ HREM images of these phases show the existence of "point defects" which can be correlated to clustering phenomena, i.e., to a local ordering of the Mn(III) or Mn(IV) species, so that a variation of the Mn−O distances around the manganese atoms would be involved. This is illustrated in Figure 7a where the bright dots are correlated to the positions of Pr, Ca, Sr and the smaller ones to Mn atom. Then we notice that contrary to the (Ln, A) sites, the intensity of the spots corresponding to the Mn sites varies considerably within a limited area (see darker dots indicated by white arrows). This local variation of the contrast (Figure 7b) can be easily simulated (Figure 7c−e) by considering $CaMn^{IV}O_3$ and $PrMn^{III}O_3$ "clusters" in which the Mn−O distance varies significantly, depending on the manganese charge. Thus, local charge clustering is demonstrated in these materials from HREM observations.

Charge Ordering Phenomena: The Manganites $Ln_{0.5}A_{0.5}MnO_3$

The manganites $Ln_{0.5}A_{0.5}MnO_3$ also exhibit CMR properties as shown for the first time by Tomioka et al.[14] for $Pr_{0.5}Sr_{0.5}MnO_3$. But the latter differs from the $Ln_{0.7}A_{0.3}MnO_3$ phase with $\langle r_A \rangle > 1.18$ Å by the existence

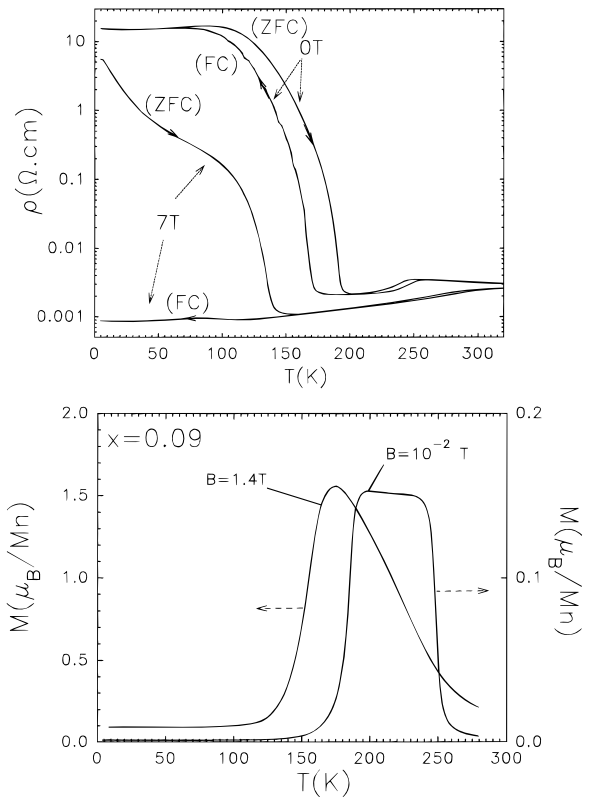

Figure 9. (a, top) $\rho(T)$ curves and (b, bottom) $M(T)$ curves of $Pr_{0.5}Sr_{0.41}Ca_{0.09}MnO_3$.

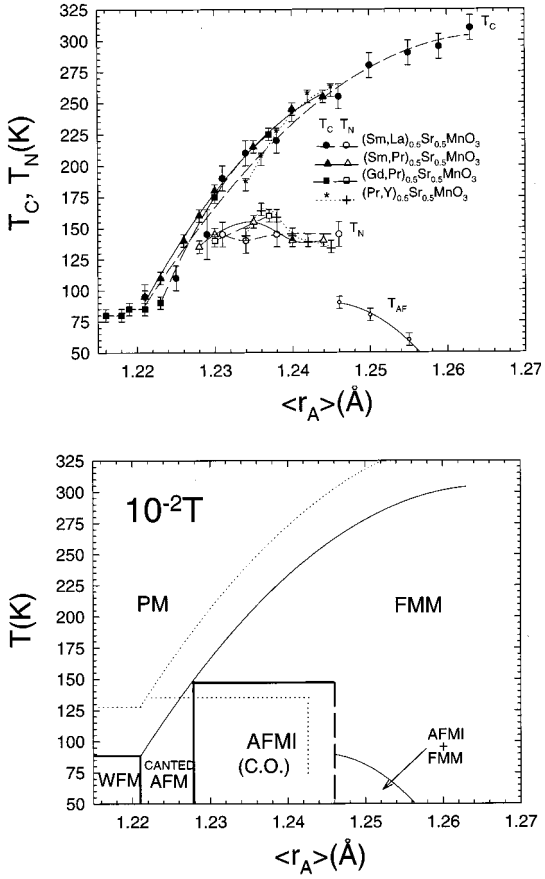

Figure 10. (a, top) $\langle r_A \rangle$ dependence of both T_C and T_N for the $(Ln,Ln')_{0.5}Sr_{0.5}MnO_3$ samples. (b, bottom) Schematic magnetic phase diagram function of cationic size and temperature of the manganites $Ln_{0.5}Sr_{0.5}MnO_3$ established for 100 G. Dotted lines would correspond to higher magnetic field values.

of two transitions at 270 and 140 K, clearly visible on the $\rho_0(T)$ curve (Figure 8a), so that a metallic state is sandwiched between two insulating states. These two metal−insulator transitions coincide with two magnetic transitions, as shown from the $M(T)$ curve registered in a magnetic field of 100 G (Figure 8b). Consequently, one observes a PMI to FMM transition at $T_C = 250$ K such as that for $Ln_{0.7}A_{0.3}MnO_3$ manganites with similar T_C, but contrastingly there exists a FMM to AFM (antiferromagnetic) transition at a lower temperature, $T_N = 140$ K.

The application of a magnetic field induces a decrease of the FMM−AFMI transition temperature, as shown from the $R(T)$ curve at 7 T (Figure 8a). However, the R_0/R_H reaches only 20 at 60 K under 7 T (Figure 8a).

Such as those for the $Ln_{0.7}A_{0.3}MnO_3$ phases, the magnetotransport properties of these manganites are strongly influenced by the size of the A-site cations. The study of the oxides $Pr_{0.5}Sr_{0.5-x}Ca_xMnO_3$[39] and $Pr_{0.5-x}Y_xCa_{0.5}MnO_3$[40] has indeed shown that the temperature T_N corresponding to the FMM−AFMI transition tends to decrease as the average ionic radius $\langle r_A \rangle$, increases; on the contrary, T_C, which characterizes the PMI−FMM transition, increases significantly with $\langle r_A \rangle$, such as that for the $Ln_{0.7}A_{0.3}MnO_3$ manganites. Clearly, the FMM state is progressively reduced as $\langle r_A \rangle$ decreases, at the benefit of the PMI and AFMI states, so that there exists a $\langle r_A \rangle$ value below which the FMM state tends to disappear.

As pointed out above, the shape of the $\rho(T)$ curve is modified on applying a magnetic field. Correspondingly the shape of the $M(T)$ curve is also modified. This is illustrated for $Pr_{0.5}Sr_{0.41}Ca_{0.09}MnO_3$ (Figure 9). The magnetoresistance effect observed for these compounds is much smaller than that observed for the $Ln_{0.7}A_{0.3}MnO_3$ oxides. It must be emphasized that the average size of the A-site cation also affects the amplitude of the CMR effect: compare for instance the maximum RR of 17 obtained for $Pr_{0.5}Sr_{0.5}MnO_3$ (Figure 8a) with the RR of 10 000 observed for $Pr_{0.5}Sr_{0.41}Ca_{0.09}MnO_3$ (Figure 9a).

In a similar way to $Ln_{0.7}A_{0.3}MnO_3$ oxides, plotting T_C and T_N versus $\langle r_A \rangle$ allows magnetic phase diagrams to be established[32] as shown on Figure 10 for the $(Ln,Ln')_{0.5}Sr_{0.5}MnO_3$ series. Note that T_C varies much more dramatically than T_N, which remains nearly constant. The AFM state is only observed in a rather short $\langle r_A \rangle$ range (1.228−1.246 Å). For larger A-site cations ($\langle r_A \rangle$ > 1.246 Å), the FMM state is favored and only weak AFM interactions remain below T_{AF} (Figure 10a). On the lower $\langle r_A \rangle$ side, i.e., below the limit 1.228 Å, the FMM state observed between the T_C and T_N branches disappears. The different magnetic states are schematically presented on Figure 10b, where it can be seen that below $\langle r_A \rangle = 1.228$ Å, the "T_C boundary" separates a canted AFM region from the PMI one as $\langle r_A \rangle$ decreases. For even smaller $\langle r_A \rangle$ values the samples become insulators with weak ferromagnetism (WFMI) below T_C (≅90 K).

In fact the comparison of the $(Ln,Ln')_{0.5}Sr_{0.5}MnO_3$ (Figure 10) series with the $Pr_{0.5}(Sr,Ca)_{0.5}$ oxides (Figure 11) shows that the average size $\langle r_A \rangle$ is not the only factor which governs T_C and T_N in these oxides. T_C does not increase so abruptly for the "$Pr_{0.5}(Sr,Ca)_{0.5}$" oxides

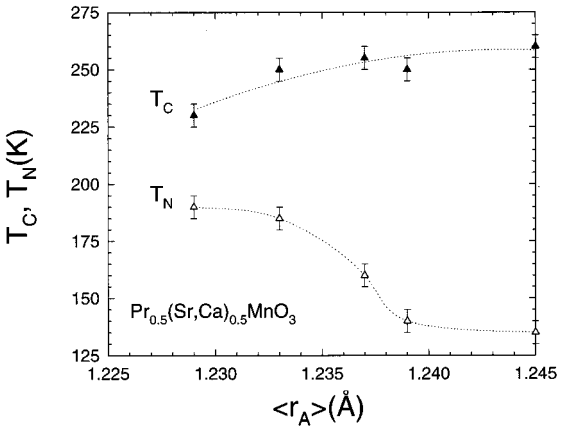

Figure 11. $\langle r_A \rangle$ dependence of both T_C and T_N for $Pr_{0.5}(Sr,Ca)_{0.5}MnO_3$ perovskites.

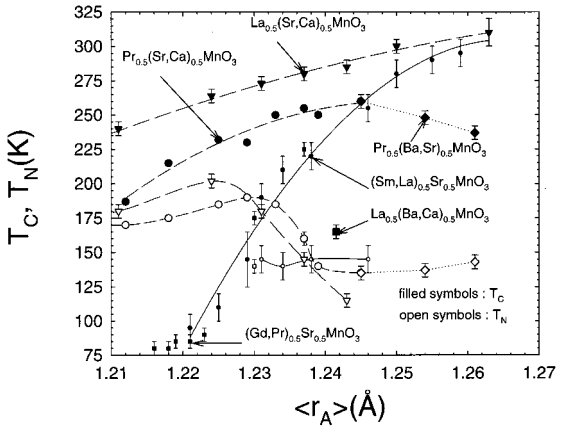

Figure 12. $\langle r_A \rangle$ dependence of T_C and T_N for six series of composition $(Ln,Ln')_{0.5}(Sr,Ca)_{0.5}MnO_3$.

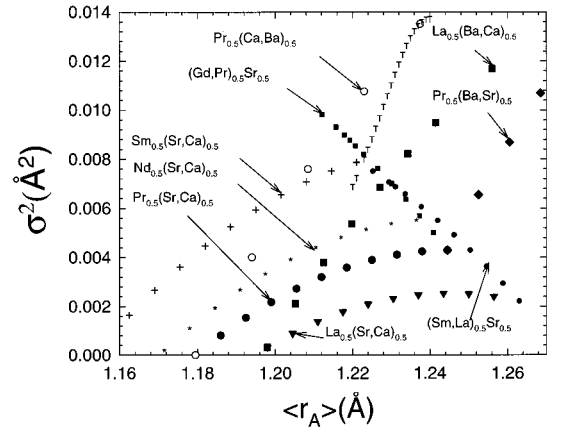

Figure 13. $\langle r_A \rangle$ dependence of the variance σ^2 for different CO series.

(Figure 11) as for the "$(Ln,Ln')_{0.5}Sr_{0.5}$" phases, and T_N decreases more severely down to 135 K as $\langle r_A \rangle$ increases. This different behavior is in fact due to the size difference between the different cations that are located on the A-sites. This apparent discrepancy is further illustrated in Figure 12, where T_C and T_N versus $\langle r_A \rangle$ are reported for different $(Ln,Ln')_{0.5}(Ca,Sr)_{0.5}MnO_3$ series of different σ^2 values. To understand these results, one must consider the σ^2 ($\langle r_A \rangle$) diagram of the corresponding compounds (Figure 13). From this diagram it is clear that σ^2 and $\langle r_A \rangle$ are not unequivocally related, as shown for instance by comparing the $Pr_{0.5}(Sr,Ca)_{0.5}$-MnO_3 and $(Gd,Pr)_{0.5}Sr_{0.5}MnO_3$ series. For the first one, σ^2 increases with $\langle r_A \rangle$, whereas for the second one the opposite is observed. As a consequence, a new magnetic diagram σ^2 ($\langle r_A \rangle$) (Figure 14) can be established in which four regions can be distinguished: weak ferromagnetic (WFM), ferromagnetic (FM), and two other regions in which charge ordering phenomena take place, labeled CO I and CO II. The charge ordered compounds are presumed to correspond to a 1:1 ordering of the Mn^{3+} and Mn^{4+} species in the structure, influencing dramatically the magnetotransport properties. As a result the first type of charge ordered manganite (CO I) observed for large sizes of the interpolated cations (1.21−1.26 Å) exhibit two transitions, AFMI−FMM and FMM−PMI, whereas the second type of charge ordered phases (CO II), observed for the smallest $\langle r_A \rangle$ values (<1.19 Å) and not too high σ^2 values (σ^2 < 0.002 Å^2), exhibit only an AFMI−PMI transition. It is remarkable that for the CO I type, the larger $\langle r_A \rangle$ is, the wider is the σ^2 range, indicating that the charge ordering becomes less sensitive to the size mismatch when the size of the A cation increases; nevertheless there exist critical σ^2 values below which FMM−PMI transitions are not seen; i.e., the FMM state does not exist. In contrast, for CO II type phases, charge ordering tends to disappear rapidly as σ^2 increases (dashed region on Figure 14), so that WFM or FM states are induced. Clearly, such a diagram emphasizes the important role of both, the size of the A cations and their mismatch on the magnetotransport properties.[41] All attempts to interpret these properties on the basis of the $\langle r_A \rangle$ effect only, without considering σ^2, are doomed to failure.

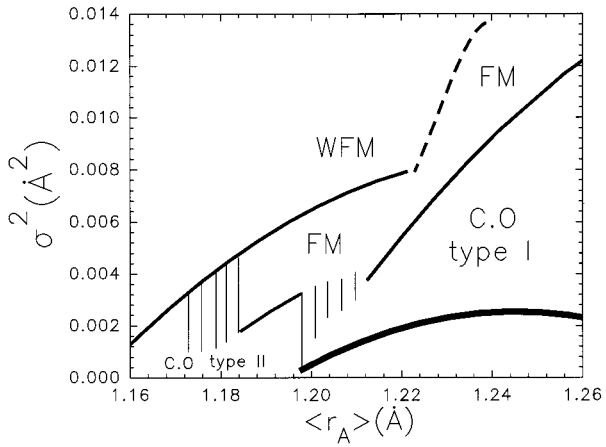

Figure 14. Magnetic phase diagram in the σ^2−$\langle r_A \rangle$ plane of $Ln_{0.5}A_{0.5}MnO_3$ phases.

The nature of charge ordering, and its relationships with magnetotransport properties, is a very important issue for the understanding of the various magnetic transitions but is so far not well-understood. This is illustrated by the behavior of the manganite $Pr_{0.5}Sr_{0.5}$-MnO_3. The crystal chemistry of this phase is complex and still subject to controversy. The room temperature form of this phase was solved in the *Pnma* space group by Knizek et al.[42] and by Kawano et al.,[43] whereas Argyriou et al.[44] solved it in the space group *F*4/*mmc*. The recent NPD study of this manganite versus temperature[45] confirms the structure of the room temperature form found by Argyriou et al., although a different cell "$a_p\sqrt{2} \times 2a_p \times a_p\sqrt{2}$" space group, *I*4/*mcm*, is used. But the first important point concerns the existence of

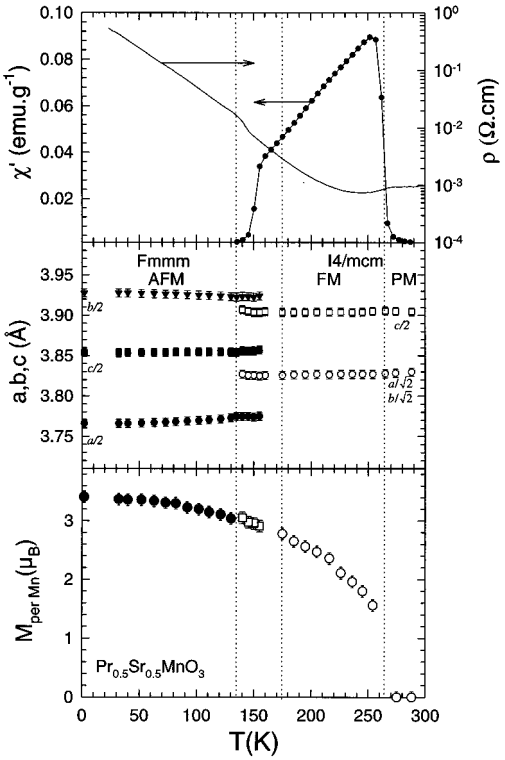

Figure 15. (a) Dependence of χ' (left axis) and ρ (right axis). (b) T dependence of the cell parameters. (c) T dependence of the ferromagnetic component in the *I*4/*mcm* structure and of the antiferromagnetic component in the *Fmmm* structure for $Pr_{0.5}Sr_{0.5}MnO_3$.

a structural transition at low temperature which coincides exactly with the FMM−AFMI transition at 140 K, as shown by comparing the $\chi'(T)$ and $\rho(T)$ curves with the structural evolution (Figure 15). The second point is that no structural transition accompanies the FMM−PMI transition at 254 K according to the NPD data. The third important result is that the low-temperature form (T < 140 K), which is described in the space group *Fmmm* with a "$2a_p \times 2a_p \times 2a_p$" cell, shows only one crystallographic site for manganese. The latter result is of critical importance since it tends to demonstrate that, within the temperature range from 4 to 293 K, no ordering of the Mn^{3+} and Mn^{4+} species takes place, contrary to what was expected from the magnetic and transport measurements which suggest charge ordering phenomena at low temperature. The electron diffraction (ED) study of $Pr_{0.5}Sr_{0.5}MnO_3$[45] confirms the structural transition at 140 K and the structure of the low-temperature form. In contrast, an apparent contradiction is obtained about the room temperature form, between ED and NPD. In ED one observes reflection conditions compatible with the space group *Imma* and not with *I*4/*mcm* deduced from NPD data. Moreover all attempts to solve the room temperature structure in the *Imma* group from NPD data are unsucessful. This different behavior might be due to the different experimental conditions (as for instance the low oxygen pressure in the electron microscope). The work done on the lattice parameters by X-ray data refinement and the bond length Mn−O at the molecular level obtained by microscopic Raman and FTIR measurements should offer a better elucidation to the question.

It must also be emphasized that the structures described above for $Pr_{0.5}Sr_{0.5}MnO_3$ are not universal for all $Ln_{0.5}A_{0.5}MnO_3$ phases. For instance, $Nd_{0.5}Sr_{0.5}MnO_3$, which is characterized like $Pr_{0.5}Sr_{0.5}MnO_3$ by AFMI−FMM−PMI transitions, exhibits fundamentally different structures.[43] Its "high-temperature" structure (T > 140 K) is indeed *Imma* "$a_p\sqrt{2} \times 2a_p \times a_p\sqrt{2}$", involving a single tiling of the almost regular MnO_6 octahedra.[46] In this compound, the AFMI−FMM transition around 160−180 K coincides also with a structural transition. But here, again, the structure of the low-temperature AFMI phase is different from that of $Pr_{0.5}Sr_{0.5}MnO_3$: the cell is orthorhombic "$2a_p\sqrt{2} \times 2a_p \times a_p\sqrt{2}$" with *Pnmm* or $Pnm2_1$ as possible space groups. The AFMI phase exhibits two different Mn sites for $Nd_{0.5}Sr_{0.5}MnO_3$, and consequently is charge ordered contrary to $Pr_{0.5}Sr_{0.5}MnO_3$.

Doping of the Manganese Sites

Although the mechanisms that are at the origin of the CMR properties are still subject to discussion, it seems clear that the electronic structure of Mn(III) and Mn(IV) species plays a specific role. Consequently, the CMR properties should be considerably modified by doping the Mn sites with various elements.

The substitution of trivalent elements (M = Al, Ga, In, Fe) or tetravalent elements (Ti, Sn) or divalent elements (Mg) for manganese in the CMR manganite $Pr_{0.7}Ca_{0.2}Sr_{0.1}MnO_3$ decreases T_C but in contrast increases significantly and even dramatically the CMR effect.[47−49] For instance $Pr_{0.7}Ca_{0.2}Sr_{0.1}Mn_{0.98}Mg_{0.02}MnO_3$ exhibits a R_0/R_{7T} at 4×10^5 at 70 K,[49] whereas from the undoped phase $Pr_{0.7}Ca_{0.2}Sr_{0.1}MnO_3$ RR reaches only 230 at 150 K. This effect is not limited to the praseodymium phase; it is indeed similarly observed for other lanthanides. This is illustrated by $Sm_{0.56}Sr_{0.44}Mn_{1-x}Fe_xO_3$,[50] for which R_0/R_{7T} reaches 8×10^5 at 55 K for $x = 0.03$ against 100 at 130 K for the undoped phase $Sm_{0.56}Sr_{0.44}MnO_3$.

Very different behavior is observed for the doped manganites $Pr_{0.5}Sr_{0.5}Mn_{1-x}M_xO_3$ with M = Al, Ga, In, Ti, Sn, Mg. Doping with divalent (Mg) or trivalent elements (Al, Ga, In) increases the AFMI and PMI states at the expense of the FMM state. Contrariwise doping with tetravalent elements (Ti, Sn) tends to suppress the AFMI state, whereas the FMM−PMI transition still exits.

The most spectacular effect is obtained by doping the Mn site of the insulator $Pr_{0.5}Ca_{0.5}MnO_3$ by Cr, Co, or Ni. It is well-known that the manganites of the series $Pr_{1-x}Ca_xMnO_3$ remain insulating for any x without a magnetic field,[51−57] due to the too small size of the interpolated cation (Pr, Ca). For $x \cong 0.5$, the charge ordering between Mn(III) and Mn(IV) species is so strong that it prevents the appearance of the I−M transition even under a magnetic field of 7 T. The doping of the Mn site of this phase with chromium, cobalt, or nickel leads to a rapid disappearance of the charge ordering.[58,59] This is illustrated by the $R(T)$ curves (Figure 16a) and $M(T)$ curves (Figure 16b) of the series $Pr_{0.5}Ca_{0.5}Mn_{1-x}Cr_xO_3$. The fact that charge ordering vanishes by doping with a foreign element is not particular to Cr, Co, or Ni: it is also observed for the manganites $Pr_{0.5}Ca_{0.5}Mn_{1-x}M_xO_3$ with M = Fe, Al, Ga, Ti.[60] But most important is the fact that this "Cr, Co, or Ni" doping induces a resistance peak characteristic

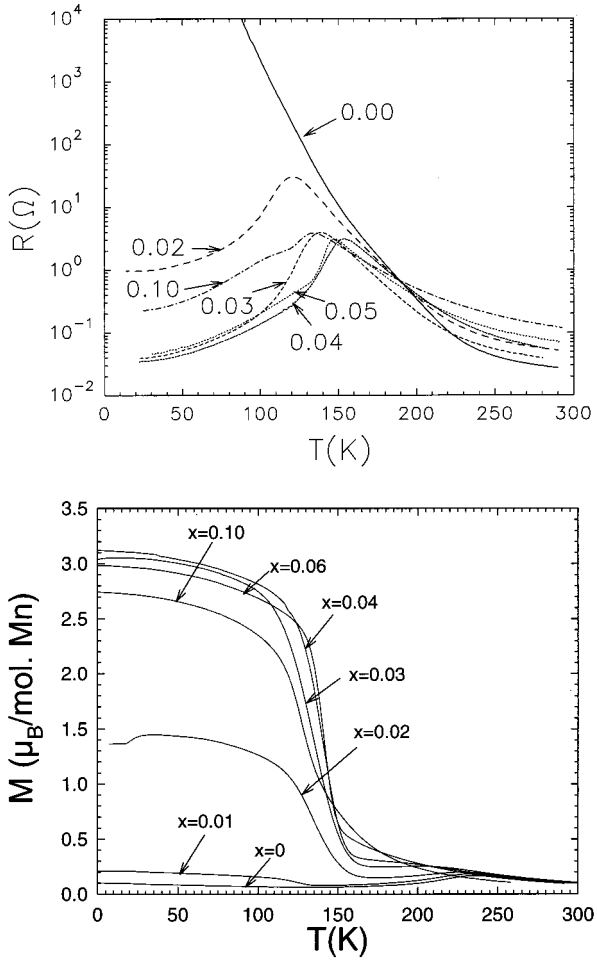

Figure 16. $R(T)$ (a, top) and $M(T)$ (b, bottom) curves for the series $Pr_{0.5}Ca_{0.5}Mn_{1-x}Cr_xO_3$.

of an I−M transition as T decreases (Figure 16a). This behavior is very different from that observed for other manganites $Pr_{0.5}Ca_{0.5}Mn_{1-x}M_xO_3$, that remain insulators, whatever M = Fe, Al, Ga, Ti and whatever x. Such an I−M transition is remarkable since it has never been observed to date in manganites with a small average size of the A-site cation. Another remarkable feature concerns the transition temperature T_{max} of the Cr-doped phases (Figure 16a) which increases significantly as the chromium content increases up to $T_{max} = 150$ K for $x = 0.04$ and then decreases for $x > 0.04$. The $M(T)$ curves (Figure 16b) corroborate the $R(T)$ curves. One indeed observes the appearance of a ferromagnetic contribution at low temperature by doping with Cr, in contrast to the undoped phase which is antiferromagnetic at those temperatures. Note the rapid increase of the magnetic moment as x increases, reaching 3−3.10 μ_B for x ranging from 0.03 to 0.06; simultaneously, T_C increases to 150 K as x increases to $x = 0.06$. Then, T_C and ferromagnetism tend to decrease as x increases beyond $x = 0.06$, as shown for the $x = 0.10$ sample that exhibits a T_C of 125 K and a magnetic moment of 2.75 μ_B at 4.2 K. Very similar behaviors are observed for cobalt and nickel, except that the maximum value of the magnetic moment is significantly smaller than for chromium. This transition from an insulator to a ferromagnetic metal suggests that the so doped samples exhibit colossal magnetoresistance properties. The induced CMR effect is indeed spectacular, as shown by

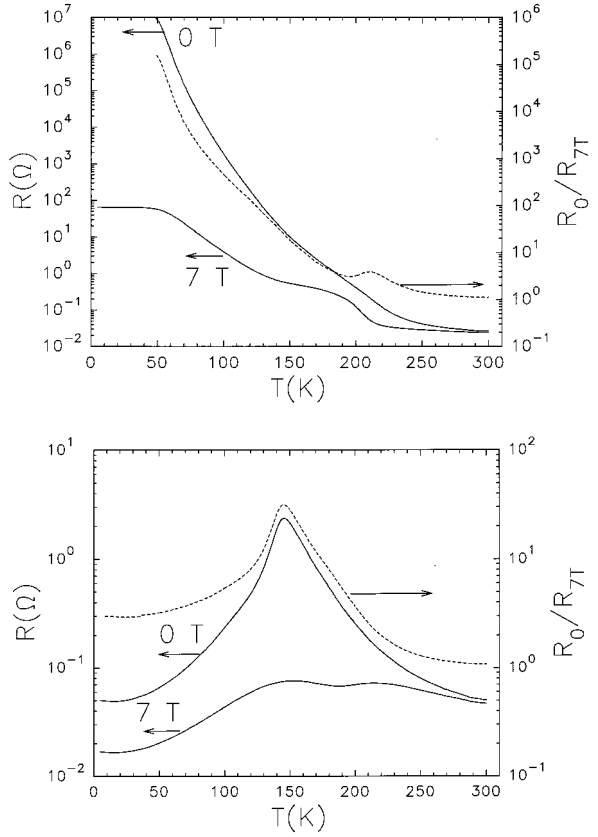

Figure 17. $R_0(T)$, $R_{7T}(T)$ and $R_0/R_{7T}(T)$ curves for $Pr_{0.5}Ca_{0.5}Mn_{1-x}Cr_xO_3$ samples: $x = 0.01$ (a) and $x = 0.05$ (b).

comparing the undoped $Pr_{0.5}Ca_{0.5}MnO_3$ manganite that is not magnetoresistant even under 7 T with the Cr doped manganites $Pr_{0.5}Ca_{0.5}Mn_{1-x}Cr_xO_3$ (Figure 17). For very weak doping levels, i.e., $x = 0.01$, that correspond to insulators in zero magnetic field, one observes high-resistance ratios of 3×10^4 (Figure 17a) at 60 K, although charge ordering has not completely disappeared. It is remarkable that as soon as the doped phase exhibits an I−M transition in a zero magnetic field, the maximum RR value decreases significantly, following the T_{max} value: a RR value of 30 is observed for the $x = 0.05$ (Figure 17b) Cr-doped phase at a T_{max} value of 145 K. It is worthy of note that, among these three dopants, cobalt exhibits the highest resistance ratios with RR $\sim 3 \times 10^6$ at 60 K under 7 T for $Pr_{0.5}Ca_{0.5}Mn_{0.99}Co_{0.01}O_3$.

The possibility of applying such an effect to other perovskites $Ln_{0.5}Ca_{0.5}MnO_3$ with a smaller lanthanide (Ln) has been demonstrated for the series $Ln_{0.5}Ca_{0.5}Mn_{1-x}Ni_xO_3$.[59] Nevertheless, it is observed that the ability to suppress charge ordering decreases as the size of Ln^{3+} decreases from Pr^{3+} to Sm^{3+}. In the same way, the difficulty to induce an I−M transition increases from Pr^{3+} to Sm^{3+}.

Electron Doped Manganites $Ca_{1-x}Ln_xMnO_3$ and $Ca_{1-x}Th_xMnO_3$

In contrast to the hole doped manganites, very few investigations have been performed on the electron doped manganites, i.e., corresponding to Mn(IV) rich perovskites. Such compounds should be of great interest if one considers the magnetic and transport proper-

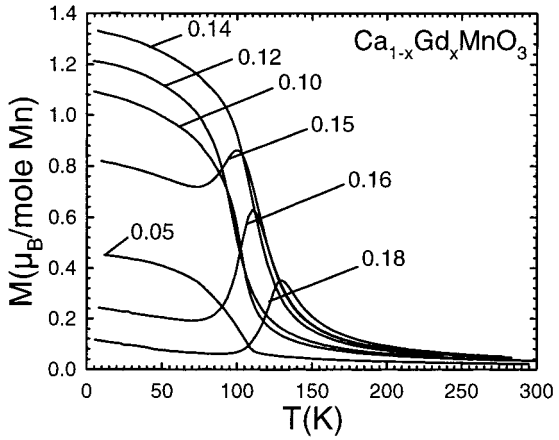

Figure 18. T dependence of the magnetization (M), registered under 1.45 T, for different compositions $Ca_{1-x}Gd_xMnO_3$ samples (x values are labeled on the graph).

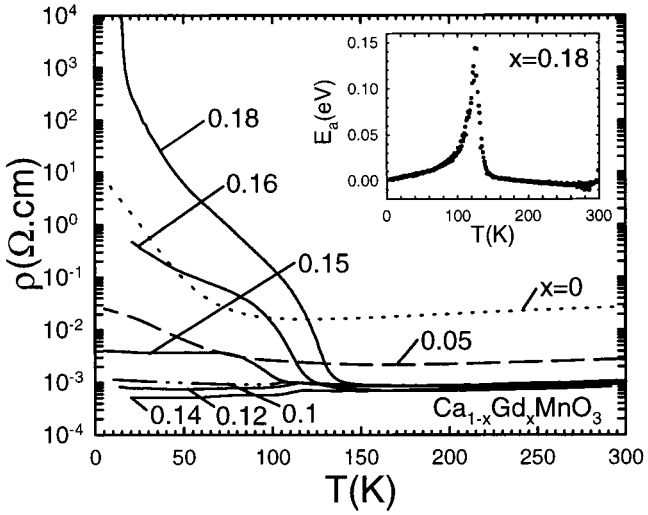

Figure 19. T dependence of the resistivity (ρ) for the same compounds. Inset: Activation energy versus T for $x = 0.18$.

ties of the perovskites $Ca_{1-x}Bi_xMnO_3$, with x ranging from 0.1 to 0.25.[61−64] Among the latter, the discovery of ferromagnetism and large magnetoresistance for $x = 0.125$ by Chiba et al.[64] suggests the possibility of inducing CMR properties in Mn(IV) rich manganites, although the resistance ratio of these materials remains small, compared to the hole doped manganites; i.e., typically, $R_0/R_{7T} \sim 3$ at 50 K. In the same way, the substitution of a trivalent rare earth Eu(III) for calcium in $CaMnO_3$ has been shown by Troyanchuk et al.[65] to induce magnetoresistance. But here again the resistivity ratio remains small $\rho_0/\rho_{12T} \sim 4$ at 30 K.

Taking into consideration these results, and the fact that the CMR properties may be highly sensitive to the carrier concentration, as demonstrated for the hole doped manganites, the manganites $Ca_{1-x}Ln_xMnO_3$ have been reinvestigated by varying x by steps of 0.01, in the range $0 < x \leq 0.20$ for Ln = Pr, Nd, Sm, Eu, Gd, Ho.[66−67]

Two important results can be evidenced from this study:

(i) For low x values ($0 < x < 0.14$ for Ln = Gd), a ferromagnetic state is induced at low temperature (Figure 18), i.e., for $T < 100$ K. Concomitantly, the resistance is lowered (Figure 19), leading to a semimetallic behavior (see for instance $x = 0.10-0.12$). It is

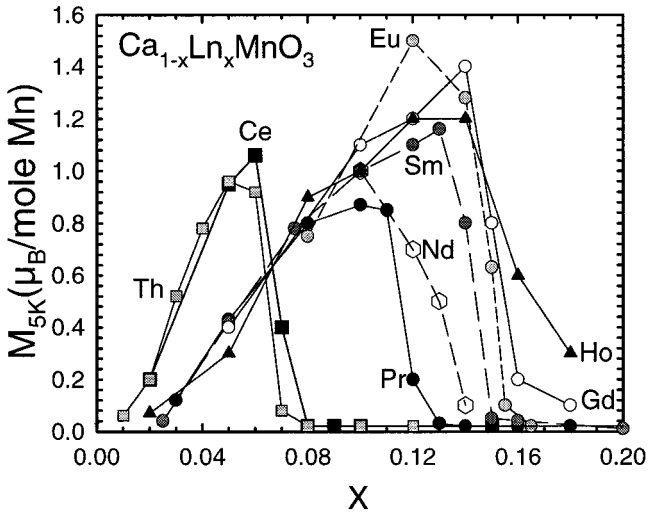

Figure 20. Magnetization, measured at 5 K (M_{5K}) versus x for different series $Ca_{1-x}Ln_xMnO_3$ (Ln = Th, Ce, Pr, Nd, Sm, Eu, Gd, Ho).

worth pointing out that the maximum magnetic moment does not overpass 1.5 μ_B in a magnetic field of 1.45 T and that it increases as the size of the lanthanide cation decreases from 0.8 μ_B for Pr to 1.5 μ_B for Eu and seems to decrease again for Ho to 1.2 μ_B (Figure 20).

(ii) For higher x values ($0.14 \leq x \leq 0.20$) a quite unusual behavior is observed, corresponding to an abrupt drop of the magnetic moment at low temperature (Figures 18 and 20) and simultaneously to a dramatic increase of the resistance (Figure 19). In fact, in this composition range, the $\rho(T)$ curve shows a transition around 100−150 K, from the semimetallic to the insulating state as T decreases. It is quite remarkable that the transition temperature T_R (see inflection point on the $\rho(T)$ curve, Figure 19) coincides with the appearance of a peak on the $M(T)$ curve (Figure 18), so that $T_{peak} \cong T_R$.

The $M(T)$ peak, also observed for $Bi_{0.2}Ca_{0.8}MnO_3$,[63−64] can be explained on the basis of electronic delocalization and localization phenomena, in accordance with the ρ-(T) curves. For low x values, introduction of electrons on the e_g* level of manganese leads to electronic delocalization and consequently favors the appearance of a FMM state at low temperature, so that the magnetic moment at 5 K increases in a first step with x. However, as x increases beyond a certain electron concentration (corresponding to $x \sim 0.12-0.14$), a localization of electrons appears (charge ordering or local charge ordering in the form of clustering), so that antiferromagnetism is favored at the expense of ferromagnetism. Consequently, ferromagnetism cannot fully develop and the saturation corresponding to a moment of 3.6 μ_B cannot be reached. Finally, the localization predominates for higher x values, and antiferromagnetism expands rapidly as x increases, so that the intensity of the peak of the $M(T)$ curves decreases abruptly (Figure 18). This interpretation agrees with the neutron diffraction study of $La_{1-x}Ca_xMnO_3$, which shows charge ordering phenomena for $x \cong 0.75$. Nevertheless, a complete structural study of all these oxides has to be performed, to determine whether the charge ordering phenomena that may appear are completely established or just involve local clusters. The $R(T)$

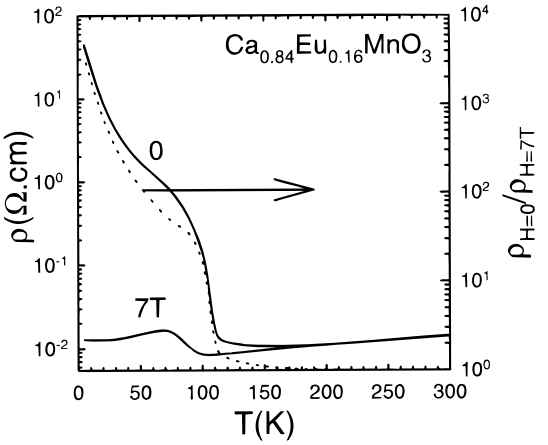

Figure 21. Temperature dependence of ρ in 0 and 7 T (left axis) and magnetoresistance ratio ρ_0/ρ_{7T} (right axis) for $Ca_{0.84}Eu_{0.16}MnO_3$.

Table 1. $\langle r_A \rangle$ (According to Shannon), σ^2, and Resistance Ratio ρ_0/ρ_{7T} for x_{opt} in Each Series $Ca_{1-x}Ln_xMnO_3$

				ρ_0/ρ_{7T}		
Ln	x_{opt}	$\langle r_A \rangle$ (Å)	σ^2 (Å^2)	at 5 K	at 50 K	at 100 K
Th	0.08	1.173	5.96×10^{-4}	50	4	3
Ce	0.08	1.167	1.88×10^{-3}	6000	5	4
Pr	0.135	1.18	1.168×10^{-7}	400	8	4.5
Nd	0.135	1.178	3.37×10^{-5}	1200	20	5
Sm	0.15	1.173	6.7×10^{-3}	1000	100	10
Eu	0.16	1.170	4.84×10^{-4}	3500	110	15
Gd	0.16	1.168	7.16×10^{-4}	500	40	10
Ho	0.16	1.163	1.57×10^{-3}	14	12	5

curves registered in a magnetic field of 7 T show the existence of a negative magnetoresistance in the whole domain for $0 < x \leq 0.20$. The low x values $0 < x \leq 0.12$, which exhibit a ferromagnetic transition, are characterized by small magnetoresistance ratios R_0/R_{7T}; i.e., RR < 3. Such an effect is comparable to that obtained for the bismuth manganite $Ca_{1-x}Bi_xMnO_3$.[64] It can be explained by the fact that the resistance in the ferromagnetic state and near the ferromagnetic state, i.e., above T_C is rather low, so that the application of a magnetic field cannot modify dramatically the resistance. In fact there exists an optimal x value for which the CMR effect is maximum. At the latter value, the competition between ferromagnetism and antiferromagnetism reaches its maximum, and, as a result, the resistance ratio is high. Above x_{opt}, the increase of antiferromagnetism tends to suppress the magnetoresistance effect, and consequently RR decreases rapidly. Thus, the x range where the material exhibits CMR effects is rather narrow. This explains why, for the series $Ca_{1-x}Eu_xMnO_3$, resistance ratios of only 4 at 30 K under 12 T were detected previously.[65] In fact, for the latter series, resistance ratios of 110 at 50 K and of 15 at 100 K are observed in a magnetic field of 7 T (Figure 21) for the value $x_{opt} = 0.16$. For each series, the x_{opt} values and the corresponding RR at three temperatures ($T = 5$, 50, and 100 K) are listed in Table 1. One observes that x_{opt} increases slightly from 0.135 for Pr to 0.16 for Eu as the size of the lanthanide decreases and then remains constant down to Ho. Correlatively, as the size of the interpolated cation decreases, the RR increases from 8 at 50 K for Pr to 110 for Eu and then decreases to 40 and 12 for Gd and Ho, respectively. It is worth pointing out that the

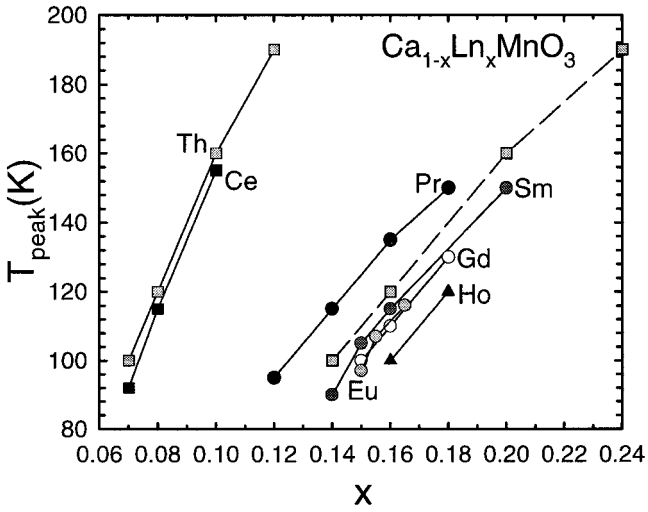

Figure 22. T_{peak}, obtained from the $M(T)$ curves, versus x, for $Ca_{1-x}Ln_xMnO_3$ and $Ca_{1-x}Th_xMnO_3$. (The dashed line corresponds to T_{peak} vs $2x$ for $Ca_{1-x}Th_xMnO_3$.)

transition temperature T_{peak} is slightly affected by the size of the lanthanide, as shown from the diagram T_{peak}-(x) for different Ln series (Figure 22). One indeed observes that for a fixed electron concentration x, the transition temperature T_{peak} decreases with the Ln size. In other words, as the mean ionic radius $\langle r_A \rangle$ of the interpolated cation decreases, a higher electron concentration is necessary to replace the FMM state at the benefit of the AFMI state. Thus, in contrast to the hole doped manganites, the stability of the FMM state increases as the size of the interpolated cation decreases. Note, however, that the size effect alone cannot explain the changes of properties that are observed, since the series $Ca_{1-x}Pr_xMnO_3$—for which $\langle r_A \rangle$ is kept constant—exhibit also the transition from a FMM to an AFMI state as x increases. It must also be emphasized that the mismatch due to the size difference between the A-site cations may also influence these properties. The latter, characterized by the variance σ^2,[34] although it increases from Pr to Ho, remains rather small for $x < 0.20$, so that its influence cannot be evaluated easily (Table 1).

At this point of the investigations it is of interest to determine the role of electron concentration upon the CMR properties of these electron doped manganites. In this respect, thorium, owing to its size which is close to that of calcium and praseodymium, is a very interesting element for substitution, since it is susceptible to introduction of twice the electrons per substituted atom than lanthanides. The $M(T)$ curves registered under 1.45 T (Figure 23) and the $\rho(T)$ curves (inset Figure 23) show that the doping of $CaMnO_3$ with thorium leads to the same effect as that obtained with trivalent lanthanides. For low x values ($x = 0.05$) ferromagnetism increases slowly with x at low temperature ($T < 100$ K) and reaches a magnetic moment of 1 μ_B at $x \cong 0.05$ (Figure 23), whereas for these compositions and temperature ranges the resistivity decreases slowly as x increases to $x = 0.04$ and then increases slightly. For $x = 0.07$ a peak appears on the $M(T)$ curves, whose intensity decreases as x increases for the larger x values ($x \sim 0.10-0.12$). As for the trivalent lanthanides, T_{peak} increases with x (Figure 23) and coincides with the transition temperature T_R deduced from the $\rho(T)$ curves

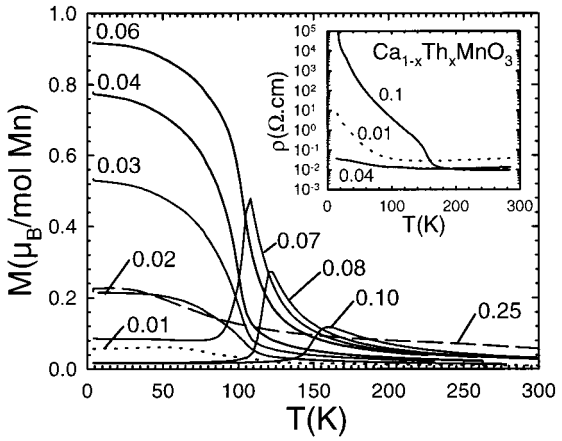

Figure 23. $M(T)$ curves for $Ca_{1-x}Th_xMnO_3$. Inset: corresponding $\rho(T)$ curves.

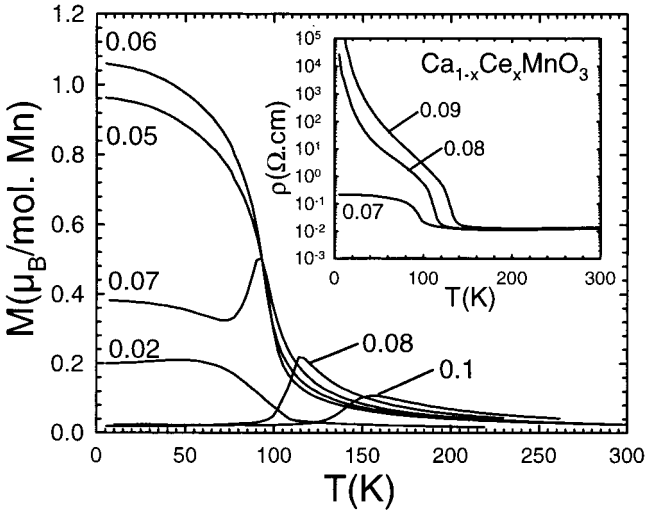

Figure 24. $M(T)$ curves for $Ca_{1-x}Ce_xMnO_3$. Inset: corresponding $\rho(T)$ curves.

which evidence also a transition from the semimetallic to semiconducting state as T decreases (inset Figure 23). Thus, the $Ca_{1-x}Th_xMnO_3$ samples exhibit, like the $Ca_{1-x}Ln_xMnO_3$ samples, a competition between ferromagnetism and antiferromagnetism at low temperature. But the most important feature concerns the evolution of T_{peak} vs x (Figure 22). One indeed observes that the transition corresponding to T_{peak} (T_R) appears for much lower thorium contents ($x \sim 0.07$ to 0.12) compared to trivalent lanthanides ($x \sim 0.135$ to 0.20). Such behavior is easily explained by the tetravalent character of thorium which introduces an electron concentration twice as high as that introduced per atom by trivalent lanthanides. Then, the behavior of Th(IV) can be better compared to that of the trivalent lanthanides by plotting T_{peak} vs $2x$, leading to the dashed line on Figure 22. From this comparison, it can be seen that, considering the electron concentration (i.e., Mn(III) concentration), the thorium substituted phases exhibit a behavior similar to that of the trivalent lanthanides. These results demonstrate that the electron concentration is a predominant factor for the magnetic and transport properties of the electron doped manganites. This behavior is also confirmed from the graph of the magnetization at 5 K versus x (Figure 20), which shows that the $M_{5K}(x)$ curves for Ln(III) doped phases are shifted by a factor 2 along x with respect to the Th substituted phase.

From this comparison between Th(IV) and Ln(III) dopants, it is possible to determine the cerium oxidation state when introduced in the perovskite matrix. The corresponding $M(T)$ curves (Figure 24) and the $\rho(T)$ curves (inset of Figure 24) clearly show that the Ce substituted phases exhibit magnetic and transport properties close to those of the thorium−manganites. At low temperature ($T < 100$ K), ferromagnetism indeed increases as x increases to $x = 0.06$ and the peak characteristic of the competition between ferromagnetism and antiferromagnetism appears exactly at $x = 0.07$, as in the case of the Th substituted phases. Correlatively the $\rho(T)$ curves (inset of Figure 24) show a transition from the semimetallic to the insulating state for the same x values. Thus, the $T_{peak}(x)$ curves (Figure 22), as well as the $M_{5K}(x)$ curves (Figure 20), are very close to those of the Th samples, i.e., are shifted by a factor $^1/_2$ along x with respect to the Ln(III) samples. These results demonstrate that cerium is tetravalent in these perovskites.

From this investigation, it is then possible to foresee that the phases $Ca_{1-x}Th_xMnO_3$ and $Ca_{1-x}Ce_xMnO_3$ will exhibit CMR properties and that the optimal x value will be close to $x_{opt} \cong 0.08$ for both series. A systematic scanning of the magnetoresistance confirms this viewpoint. Both series of oxides, Th and Ce doped compounds, exhibit CMR properties with similar RR.

Concluding Remarks

The considerable work that has been performed to date on CMR perovskite manganites shows the great potentiality of these materials. Despite the impressive number of data that have been accumulated, several issues will have to be answered in order to progress in the understanding of the mechanisms which govern the CMR. If there is no doubt that the double exchange mechanism is the basis of the CMR effect, the role of Jahn−Teller distortion is not yet clear, and accurate structural studies, especially near the transition temperatures, will have to be performed, coupling neutron diffraction and high-resolution electron microscopy. Such studies will also be of crucial importance in accounting for the charge ordering phenomena which seem to appear in several of these oxides.

The preliminary explorations that have been made these past years have allowed guidelines to be drawn for the research of new CMR materials, especially for oxides containing chromium, cobalt, and nickel. At this point of the investigations it is absolutely necessary to determine the role of the tiny structural distortions (local or long-range order) in the modification of the magnetotransport properties of these oxides versus temperature.

References

(1) von Helmolt, R.; Wecker, J.; Holzapfel, B.; Schultz, L.; Sanwer, K. *Phys. Rev. Lett.* **1993**, *71*, 2331.
(2) Chahara, K.; Ohno, T.; Kasai, M.; Kozono, Y. *Appl. Phys. Lett.* **1993**, *63*, 1990.
(3) Rao, C. N. R.; Cheetham, A. K.; Mahesh, R. *Chem. Mater.* **1996**, *8*, 2421.
(4) Raveau, B.; Maignan, A.; Martin, C.; Hervieu, M. In *Colossal magnetoresistance and related properties*; Rao, C. N. R., Raveau, B., Eds.; World Scientific: Singapore, 1998.

(5) Tokura, Y.; Urushibara, A.; Moritomo, Y.; Arima, T.; Asamitsu, A.; Kido, G.; Furukawa, N. *J. Phys. Soc. Jpn.* **1994**, *63*, 3931.
(6) Ju, H. L.; Kwon, C.; Li, Q.; Greene, R. L.; Venkatesan, T. *Appl. Phys. Lett.* **1994**, *65*, 2108.
(7) Jin, S.; Tiefel, T. H.; Mc Cormack, M.; Fastnacht, R. A.; Ramesh, R.; Chen, L. H. *Science* **1994**, *264*, 413.
(8) Manoharan, S. S.; Vasanthacharya, N. Y.; Hegde, M. S.; Satyalakshmi, K. M.; Prasad, V.; Subramanyam, S. V. *J. Appl. Phys.* **1994**, *76*, 3923.
(9) Mahesh, R.; Mahendiran, R.; Raychaudhuri, A. K.; Rao, C. N. R. *J. Solid State Chem.* **1995**, *114*, 297; **1995**, *120*, 204.
(10) Mahendiran, R.; Mahesh, R.; Raychaudhuri, A. K.; Rao, C. N. R. *Solid State Commun.* **1995**, *94*, 515.
(11) Inoue, J.; Maekawa, S. *Phys. Rev. Lett.* **1995**, *74*, 3407.
(12) Kuwahara, H.; Tomioka, Y.; Asamitsu, A.; Moritomo, Y.; Tokura, Y. *Science* **1995**, *270*, 961.
(13) Caignaert, V.; Maignan, A.; Raveau, B. *Solid State Commun.* **1995**, *95*, 357.
(14) Tomioka, Y.; Asamitsu, A.; Moritomo, Y.; Kuwahara, H.; Tokura, Y. *Phys. Rev. Lett.* **1995**, 56.
(15) Urushibara, A.; Morimoto, Y.; Arima, T.; Asamitsu, A.; Kido, G.; Tokura, Y. *Phys. Rev. B* **1995**, 14103.
(16) Maignan, A.; Simon, Ch.; Caignaert, V.; Raveau, B. *Solid State Commun* **1995**, *96*, 623.
(17) Maignan, A.; Caignaert, V.; Simon, Ch.; Hervieu, M.; Raveau, B. *J. Mater. Chem.* **1995**, *5*, 1089.
(18) Raveau, B.; Maignan, A.; Simon, Ch. *J. Solid State Chem.* **1995**, *117*, 424.
(19) Zener, C. *Phys. Rev.* **1951**, *81*, 440.
(20) de Gennes, P. G. *Phys. Rev.* **1960**, *118*, 141.
(21) Goodenough, J. B. *Phys. Rev.* **1955**, *100*, 564.
(22) Millis, A. J.; Littlewood, P. B.; Shraiman, B. I. *Phys. Rev. Lett.* **1995**, *74*, 5144.
(23) Maignan, A.; Simon, Ch.; Caignaert, V.; Raveau, B. *J. Magn. Magn. Mater.* **1996**, *152*, L5.
(24) Maignan, A.; Simon, Ch.; Caignaert, V.; Raveau, B. *Z. Phys. B* **1996**, *99*, 305.
(25) Hejtmanek, J.; Jirak, Z.; Sedmidubsky, D.; Maignan, A.; Simon, Ch.; Caignaert, V.; Martin, C.; Raveau, B. *Phys. Rev. B* **1996**, *54*, 11947.
(26) Millange, F.; Maignan, A.; Caignaert, V.; Simon, Ch.; Raveau, B. *Z. Phys. B* **1996**, *101*, 169.
(27) Fontcuberta, J.; Martinez, B.; Seffar, A.; Pinol, S.; Garcia-Munoz, J. L.; Obradors, X. *Phys. Rev. Lett.* **1996**, *76*, 1122.
(28) Radaelli, P. G.; Marezio, M.; Hwang, H. Y.; Cheong, S. W. *J. Solid State Chem.* **1996**, *122*, 444.
(29) Hwang, H. Y.; Cheong, S. W.; Radaelli, P. G.; Marezio, M.; Batlogg, B. *Phys. Rev. Lett.* **1995**, *75*, 914.
(30) Maignan, A.; Simon, Ch.; Caignaert, V.; Raveau, B. *J. Appl. Phys.* **1996**, *79*, 7891. Mahendiran, R.; Mahesh, R.; Raychaudhuri, A. K.; Rao, C. N. R. *Phys. Rev. B* **1996**, *53*, 12160.
(31) Hwang, H. Y.; Cheong, S. W.; Radaelli, P. G.; Marezio, M.; Batlogg, B. *Phys. Rev. Lett.* **1995**, *75*, 914.
(32) Damay, F.; Maignan, A.; Martin, C.; Raveau, B. *J. Appl. Phys.* **1997**, *81*, 1372.
(33) Kumar, N.; Rao, C. N. R. *J. Solid State Chem.* **1997**, *129*, 362.
(34) Rodriguez-Martinez, L. M.; Attfield, J. P. *Phys. Rev. B* **1996**, *54*, R15622.
(35) Caignaert, V.; Suard, E.; Maignan, A.; Simon, Ch.; Raveau, B. *C. R. Acad. Sci.* **1995**, *321*, 515.
(36) Argyriou, D. N.; Mitchell, J. F.; Potter, C. D.; Hinks, D. G.; Jorgensen, J. D.; Bader, S. D. *Phys. Rev. Lett.* **1996**, *76*, 3826.
(37) Hervieu, M.; Van Tendeloo, G.; Caignaert, V.; Maignan, A.; Raveau, B. *Phys. Rev. B* **1996**, *53*, 14274.
(38) Caignaert, V.; Suard, E.; Maignan, A.; Simon, Ch.; Raveau, B. *J. Magn. Magn. Mater.* **1996**, *153*, L260.
(39) Wolfman, J.; Simon, Ch.; Hervieu, M.; Maignan, A.; Raveau, B. *J. Solid State Chem.* **1996**, *123*, 413.
(40) Wolfman, J.; Maignan, A.; Simon, Ch.; Raveau, B. *J. Magn. Magn. Mater.* **1996**, *159*, L299.
(41) Damay, F.; Maignan, A.; Martin, C.; Raveau, B. *J. Appl. Phys.* **1997**, *81*, 1372.
(42) Knizek, K.; Jirak, Z.; Pollert, E.; Zounova, F.; Vratislav, S. *J. Solid State Chem.* **1992**, *100*, 292.
(43) Kawano, H.; Kajimoto, R.; Yoshizawa, H.; Tomioka, Y.; Kuwahara, H.; Tokura, Y. *Phys. Rev. Lett.* **1997**, *78*, 4253.
(44) Argyriou, D. N.; Hinks, D. G.; Mitchell, J. F.; Potter, C. D.; Schultz, A. J.; Young, D. M.; Jorgensen, J. D.; Bader, S. D. *J. Solid State Chem.* **1996**, *124*, 381.
(45) Damay, F.; Martin, C.; Hervieu, M.; Maignan, A.; Raveau, B.; André, G.; Bourée, F. *J. Magn. Magn. Mater.* **1998**, *184*, 71.
(46) Laffez, P.; Van Tendeloo, G.; Millange, F.; Caignaert, V.; Hervieu, M.; Raveau, B. *Mater. Res. Bull.* **1996**, *31*, 905.
(47) Maignan, A.; Martin, C.; Raveau, B. *Z. Phys. B* **1997**, *102*, 19.
(48) Martin, C.; Maignan, A.; Raveau, B. *J. Mater. Chem.* **1996**, *6*, 1245.
(49) Maignan, A.; Raveau, B. *Z. Phys. B* **1997**, *102*, 209.
(50) Damay, F.; Maignan, A.; Nguyen, N.; Raveau, B. *J. Solid State Chem.* **1996**, *124*, 385.
(51) Jirak, Z.; Krupicka, S.; Nekvasil, V.; Pollert, E.; Villeneuve, G.; Zounova, F. *J. Magn. Magn. Mater.* **1980**, *15*, 519.
(52) Pollert, E.; Krupicka, S.; Simsa, Z.; Dlouha, M.; Vratislav, V. *J. Phys. Chem. Solids* **1982**, *43*, 1137.
(53) Jirak, Z.; Krupicka, S.; Simsa, Z.; Dlouha, M.; Vratislav, V. *J. Magn. Magn. Mater.* **1985**, *53*, 153.
(54) Yoshizawa, H.; Kawano, H.; Tomioka, Y.; Tokura, Y. *J. Phys. Soc. Jpn.* **1996**, *65*, 1043.
(55) Yoshizawa, H.; Kawano, H.; Tomioka, Y.; Tokura, Y. *Phys. Rev. B* **1995**, *52*, R13145.
(56) Tomioka, Y.; Asamitsu, A.; Moritomo, Y.; Tokura, Y. *J. Phys. Soc. Jap.* **1995**, *64*, 60.
(57) Lees, M. R.; Barratt, J.; Balakrishnan, G.; MacK. Paul, D.; Yethiraj, M. *Phys. Rev. B* **1995**, *52*, R14303.
(58) Raveau, B.; Maignan, A.; Martin, C. *J. Solid State Chem.* **1997**, *130*, 162.
(59) Maignan, A.; Damay, F.; Martin, C.; Raveau, B. *Mater. Res. Bull.* **1997**, *32*, 965.
(60) Damay, F.; Martin, C.; Maignan, A.; Raveau, B. *J. Magn. Magn. Mater.* **1998**, *183*, 143.
(61) Bokov, V. A.; Grigoryan, N. A.; Bryzhina, M. F. *Phys. Status Solidi* **1967**, *20*, 745.
(62) Bao, W.; Axe, J. D.; Chen, C. H.; Cheong, S. W. *Phys. Rev. Lett.* **1997**, *78*, 543.
(63) Murakami, T.; Shindo, D.; Chiba, H.; Kikuchi, M.; Syono, Y. *Phys. Rev.* B **1997**, *55*, 1.
(64) Chiba, H.; Kikuchi, M.; Kusaba, K.; Muraoka, Y.; Syono, Y. *Solid State Commun.* **1996**, *99*, 499.
(65) Troyanchuk, I. O.; Samsonenko, N. V.; Szymczak, H.; Nabialek, A. *J. Solid State Chem.* **1997**, *131*, 144.
(66) Martin, C.; Maignan, A.; Damay, F.; Hervieu, M.; Raveau, B. *J. Solid State Chem.* **1997**, *134*, 198.
(67) Maignan, A.; Martin, C.; Damay, F.; Raveau, B. *Chem. Mater.* **1998**, *10*, 950.

CM9801791